Available Online at http://www.journalajst.com

ASIAN JOURNAL OF SCIENCE AND TECHNOLOGY

ISSN: 0976-3376

Asian Journal of Science and Technology
Vol. 16, Issue, 10, pp. 13933-13940, October, 2025

RESEARCH ARTICLE

REMOTE SENSING MAPPING OF THE BASEMENT ROCKS OF NORTHERN KORBOL IN MOYEN CHARI PROVINCE, SOUTHERN CHAD

Mahamat Boka Ramadane[1], Baïssemia Ronang Gustave[2*], Doumnang Mbaïgane Jean Claude[3], Madjimbe Guiguindibaye[1] and Allarassem Luthian[3]

[1]Department of biologu and geology, Sarh University, Sarh Chad; [2]Department of Mining and Geological Engineering, Faculty of Life and Earth Sciences, Pala University, P.O. Box. 20, Pala, Chad; [3]Laboratory of Geology, Geomorphology and Remote Sensing, University of N'djamena/Chad

ARTICLE INFO

Article History:
Received 11th July, 2025
Received in revised form
19th August, 2025
Accepted 24th September, 2025
Published online 27th October, 2025

Key words:
Landsat-8, geological mapping, North of Korbol, Southern Chad.

***Corresponding author:**
Baïssemia Ronang Gustave

ABSTRACT

Remote sensing technology is already widely used in various geological fields such as mineralogy, lithological mapping, geomorphology and so on. In our study, it is specifically used for lithological mapping. This work aims to map rock types in the Korbol region by integrating remote sensing applications of Landsat-8 image processing (OLI), field studies and petrographic investigations. The aim of the present work is to produce a geological map of the area north of Korbol, south of the Guéra massif, due to the absence of a geological map. We used the optimal indexing factor and correlation coefficient methods to identify the most effective results from false color composite (FCC), principal component analysis (PACP) and band ratio (BR). These techniques, combined with supervised classification, enabled us to distinguish the different rock units on the basis of their spectral signatures. The results were combined with the aforementioned techniques, including principal component images (PACP1, PACP2, PACP3) and band ratio images (6/5, 4/5, 1/6 and 6/7, 6/2 and 6/5). As a result, geological mapping has been underpinned and field and laboratory petrographic studies confirmed. This approach identified six distinct lithological units, namely pyroxene amphibolite; biotite amphibolite; biotite gneiss, quartz diorite, biotite granite and biotite-amphibole granite. Landsat-8 image processing revealed that the geological basement of the northern Korbol massif is predominantly granitic. ESE-WNW to NE-SW directions and a secondary NE-SW direction are the main fracture directions in these geological formations.

Citation: ***Mahamat Boka Ramadane, Baïssemia Ronang Gustave, Doumnang Mbaïgane Jean Claude , Madjimbe Guiguindibaye, Allarassem Luthian.*** **2025.** "Remote sensing mapping of the basement rocks of northern Korbol in Moyen Chari Province, Southern Chad.", *Asian Journal of Science and Technology*, 16, (10), 13933-13940.

INTRODUCTION

The Pan-African basement rock units north of Korbol are poorly known. The basement of the study area is located south of the Sahara metacraton and was formed during the Neoproterozoic Pan-African orogeny (Abdelsalam *et al*., 2002; Sadek *et al*., 2015, 2020). Nowadays, geological mapping has been improved by the use of remote sensing techniques. However, digital satellite imagery processing algorithms play an important role in lithological discrimination, geological mapping and the detection of mineralized alteration zones (Sadek *et al*., 2015, 2020, Parsa et Pour, 2021, Safianou *et al*., 2023). The development of satellite imagery analysis techniques has improved the accuracy of explored targets (Chen *et al*. 2024; Safianou *et al*. 2023, 2024a; Zhao *et al*. 2024). In the present work, remote sensing techniques were used for lithological discrimination of basement rocks in northern Korbol, Moyen Chari province. The study area is undocumented, with no geological map. The study area is located at the southern margin of the Saharan metacraton and forms the Central African Pan-African Chain (Fig. 1a and b), which links it to the Congo Craton (Abdelsalam *et al*., 2002; Pin and Poidevin, 1987; Toteu *et al*., 2004). However, the geology of the S-SE region of Chad is relatively poorly understood due to its geographical isolation and recent sedimentary cover.

Geological framework: In Chad, the basement formations are distributed to the north by the Tibesti massif, to the east by the Ouaddaï massif, to the south-west by the Mayo Kebbi massif, to the center by the Guéra massif and to the south by the Yadé massif, also known as the Baïbokoum massif (Fig. 1b). The Yadé massif, also known as the Baïbokoum massif, lies on the southern border of Chad and extends into the Central African Republic and Cameroon. It is characterized by an abundance of syntectonic granitoids containing enclaves of metamorphic rocks intersected by late granitic intrusions (Black, 1992, Seguem *et al*. 2014, 2022, Baïssemia Ronang *et al*. 2025). This Yadé massif includes Neoproterozoic ages, notably a granite and syenite described by Mbaïtoudji (1982) and Liégeois (1992) that gave K-Ar and Rb-Sr ages on total rock of between 632 and 568 Ma. The Ouaddaï massif is composed of metasedimentary series, with mafic magmatic intercalations in the form of amphibolite (Kasser, 1995; Djerossem, 2018; Djerossem *et al*. 2020). The age of the hyperaluminous granites was constrained by U-Pb dating on zircon, giving 635 ± 3Ma for a biotite leucogranite and 613 ± 8Ma for a muscovite-garnet leucogranite. The age of the metaluminous, calc-alkaline and strongly potassic to shoshonitic series was determined at 540 ± 5Ma by U-Pb zircon dating of a biotite granite (Liégeois, 1992, Shellnut *et al*., 2020, Djerossem *et al*., 2020; De Wit *et al*., 2021). The Mayo-Kébbi domain is an elongated NE-SW unit that lies between the Centre-Cameroun and Nord-Cameroun domains. It is

distinguished from these two domains by its juvenile Neoproterozoic crust (Penaye *et al*., 2006; Pouclet *et al*., 2006; Isseini, 2011; Isseini *et al*., 2012). This domain corresponds to a magmatic arc zone that formed between 800 Ma and 550 Ma by successive collision with the Centre-Cameroun and Nord-Cameroun domains respectively (Penaye *et al*., 2006; Pouclet *et al*., 2006; Isseini, 2011). It includes the greenstone belts, the Mayo-Kébbi batholith, and post-tectonic intrusions (Kasser, 1995; Doumnang 2006; Penaye *et al*., 2006; Pouclet *et al*., 2006; Isseini, 2011, Isseini *et al*., 2012, Mbaguedjé, 2015). The Tibesti massif is made up of metasedimentary rocks and metavolcanites (Wacrenier, 1958) and a set of granoblastic amphibolites, locally migmatitic, associated with various gneisses and granitoids. Ages ranging from 1250 to 820 Ma have been obtained in the Lower Tibestian (El Makhrouf, 1988). The Upper Tibestian consists of slightly metamorphosed detrital rocks (Kasser, 1995). Various calc-alkaline intrusions dated between 600 and 530 Ma (Super-Tibestian magmatic series and Ben Ghnema batholith, Eghei magmatic series, Wadi Yebigue pluton) cut across Lower and Upper Tibestian formations (El Makhrouf, 1988; Suayah *et al*. 2006).

The Guéra massif is composed of amphibole monzonitic granite (Abou Déïa type) or highly radioactive alkaline leucocratic granite (Kasser, 1995; Kusnir, 1995; Kusnir & Moutaye, 1997; Diontar *et al*., 2020a, 2020b; Shellnut *et al*., 2020; De Wit *et al*., 2021). The metamorphic formations of the Guéra comprise the metavolcano-sedimentary series, often in enclaves within the granite and attached to the Goz Beïda group (Kasser, 1995; Diontar *et al*., 2020a). The granites near Lake Fitri are presumed to be Neoproterozoic in age. New zircon U/Pb geochronology of granitic rocks from the Guéra massif, the Lake Fitri region and the Doba Basin in southern Chad have yielded weighted mean 206Pb/238U ages of 595 ± 8 Ma to 545 ± 6 Ma (Shellnutt *et al*., 2017). In the Lac Iro area, porphyritic granites yield zircon U-Pb emplacement ages corresponding to a period of 575.3 ± 5.6 to 581.3 ± 3.8 Ma (Couzinié *et al*., 2020). The post-Pan-African cover of the study area comprises Cretaceous to Quaternary terrigenous sedimentary formations (Genik, 1993; Guiraud *et al*., 2005) that constitute sequences notably several kilometers thick, in four transtensional extensional basins (Bongor, Doba, Doseo and Salamat). Sedimentation in these basins was controlled by normal to dextral brittle deformation along crustal structures parallel to Pan-African shear zones, suggesting a strong structural legacy (Genik, 1993). Prolonged alkaline volcanic activity from the Cretaceous to the Pliocene has also been recorded in the region (Nkouandou *et al*., 2008).

MATERIALS AND METHODS

The materials and methods used and followed in the study area are illustrated in the following flow chart (Fig. 2). The cloud-free scene of Landsat 8 OLI data (path/row: 180) obtained on March 12, 2025 covering the northern Korbol region and downloaded from the United States Geological Survey website (https://earthexplorer.usgs.gov) was used to map rock units and detect lineaments. It belongs to Universal Transverse Mercator (UTM) zone 34 North, using the WGS-84 reference system. Landsat 8 OLI data consists of a collection of nine bands (bands 1-9) and two TIR (thermal infrared) bands (bands 10-11). In this study, the Landsat 8 visible and near infrared (VNIR), shortwave infrared (SWIR) and panchromatic (b8) bands were used. Principal component analysis (PCA) was applied to the spectral bands of Landsat-8 data to highlight the exposed rock units in the study area using petrography. Envi 5.3 software was used for radiometric correction on the Landsat 8 OLI bands. Radiometric calibrations and fast atmospheric corrections (QUAC) were applied to the Landsat 8 VNIR-SWIR bands for high-precision detection. Indeed, QUAC performs a more approximate atmospheric correction than other methods such as Fast Line-of-sight Atmospheric Analysis of Spectral Hypercube (FLAASH), typically producing a reflectance spectrum that lies between 10 and 15% of ground truth (Bernstein *et al*. 2012). In addition, lineaments were extracted using PCI software version 9.1 with two different datasets, namely the high-resolution digital elevation model. The rosette and lineament statistics were obtained from RockWorks software and finally the layout was done with ArcGIS 10.8 software. field campaigns collected samples on different lithological types and in the laboratory thin section making and description were carried out.

RESULTS AND DISCUSSION

Lithological mapping: As an approach to lithological discrimination, mapping frequently uses remote sensing coupled with geographic information systems (GIS).

False color combination: The color composition was generated using the VNIR-SWIR bands of Landsat 8 OLI data. As a result, the combination of bands 751, 654 and 423 of Landsat-8 OLI data was assigned as RGB images to distinguish rock formations. The resulting 751, 654 and 423 color composition image of the study area is shown in Fig. 3, where rock unit contacts are identified using their spectral reflection and absorption characteristics (Fig. 3a, b and c) from the United States Geological Survey spectral library (Clark *et al*. 1993).

Band ratios (BR): We produced a true-color composition using combinations of bands 654, 751 and 423. Band ratios are techniques that divide the radiometric value of a pixel in one band by the radiometric value of a pixel in another band (Yang'tshi *et al*., 2018, Ngambi *et al*., 2025).

Two separate BRs composed from Landsat-8 OLI data (6/5, 4/5, 1/6 and 6/7, 6/2 and 6/5) were produced to discriminate rock units in the study area. Based on the spectral properties of the weathering minerals, these BRs were assigned to the RGB combination for rock unit discrimination and mapping.

Principal component analysis: In order to map the different lithological types and deformation structures that have affected the Precambrian basement in the northern part of Korbol, we carried out a principal component analysis on the first seven (7) bands of the OLI instrument, ranging from the visible to mid-infrared 2. This resulted in 6 components (band 6 is not taken into account by the principal component analysis) CPA1, CPA2, CPA3, CPA4, CPA5 and CPA7. The statistical results show that band 1 (CPA1) has the maximum amount of decorrelated information (Fig. 4), and the first three bands provided by the principal component analysis (CPA1, CPA2 and CPA3), also show the maximum amount of information in a single image in RGB mode.

Lineament analysis: In this study, Landsat 8's panchromatic OLI band (band 7) was used for lineament extraction, which includes manual and automatic extraction processes using PCI Geomatica 2015 and ArcGIS software. Each lithological unit bears its lineament pattern, according to the lineament map and density map (Fig. 5a). The lineament rose diagram shows two structural directions (Fig. 5b): (i) a dominant ESE-WNW to NW-SE direction and (ii) a secondary NE-SW direction (Djerossem *et al*., 2024). Analysis of the lineament density map revealed that major lineaments are dominant in red tones in the northern, southern, western and central parts of the study area (Fig. 5a).

Petrography: In order to validate the results obtained from the remote sensing data, field investigations and laboratory analyses (thin section observation) were carried out, resulting in the geological map (Fig. 6). Petrographically, the study area consists of granitoids (mainly biotite-hornblende granite and biotite granite) embedded in Pan-African amphibolites (biotite amphibolite and pyroxene amphibolite) and biotite gneisses. The amphibolites and gneisses form large enclaves in the study area.

Pyroxene amphibolites: At outcrop, pyroxene amphibolite is enclosed by biotite granite or biotite-amphibole granite (Fig. 7a and b). Pyroxene amphibolite has a grano-nematoblastic texture. It consists mainly of amphibole, plagioclase and pyroxene blasts. Other mineral phases include biotite, quartz, alkali feldspar, apatite, titanite, opaque minerals and zircon.

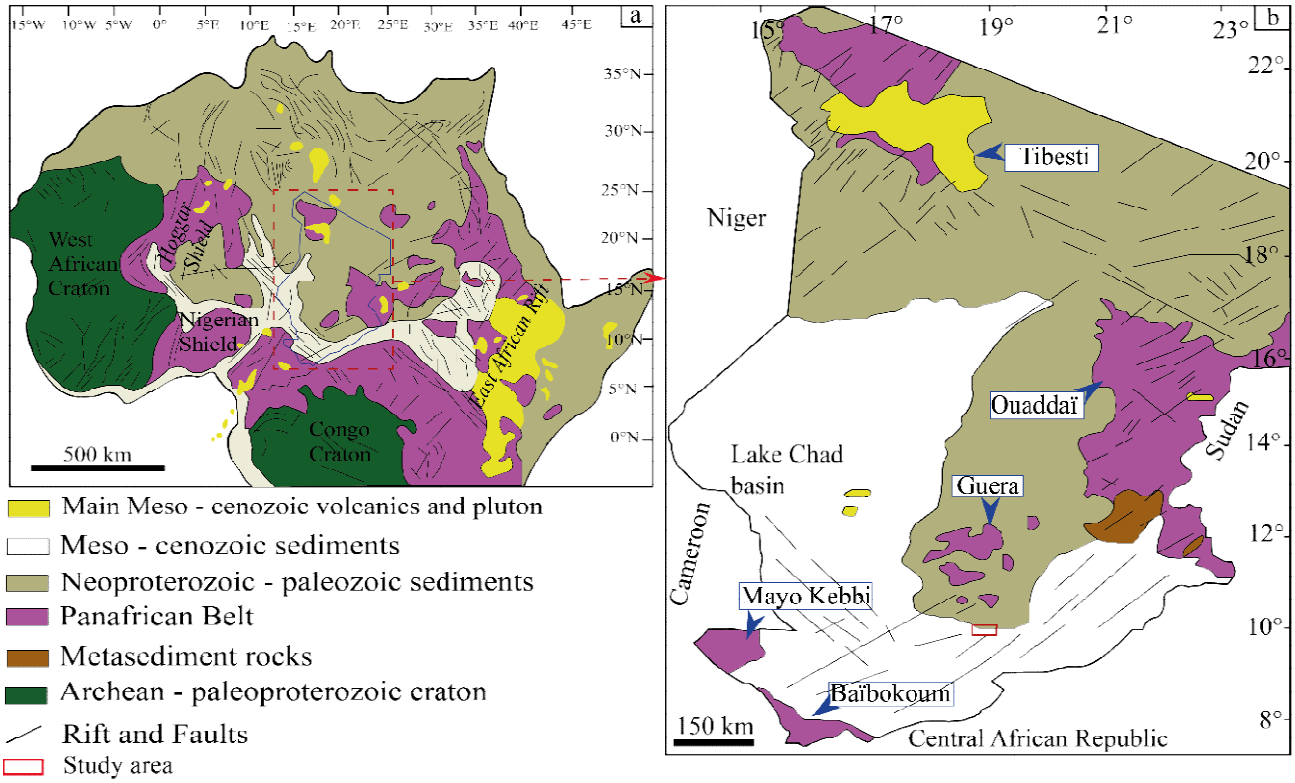

Figure 1. a) Tectonic Map of Africa, location map of Chad. The main geologic features of Africa are indicated (Kogbe, C.A. (1981); Milesi et al. (2010). b) Geological map of Chad showing the Precambrian formations

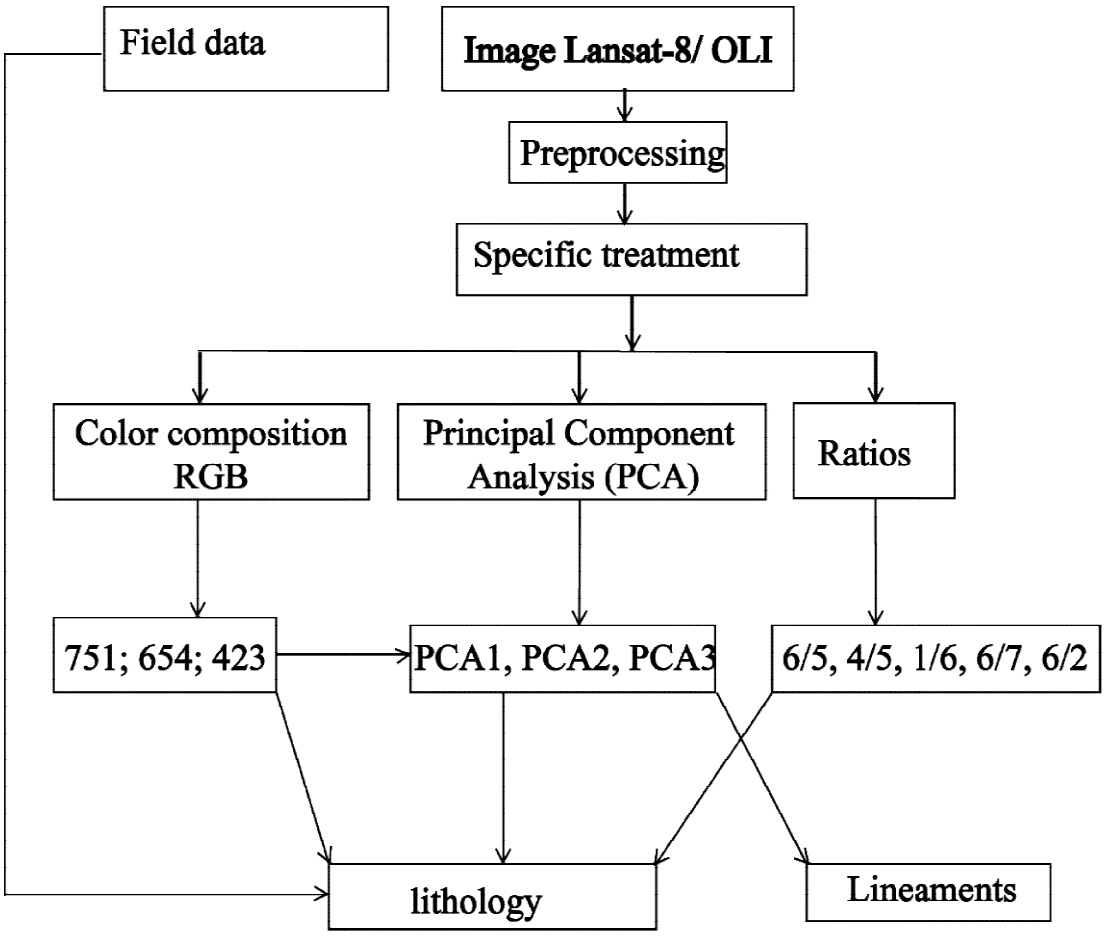

Figure 2. Landsat-8 satellite image processing techniques

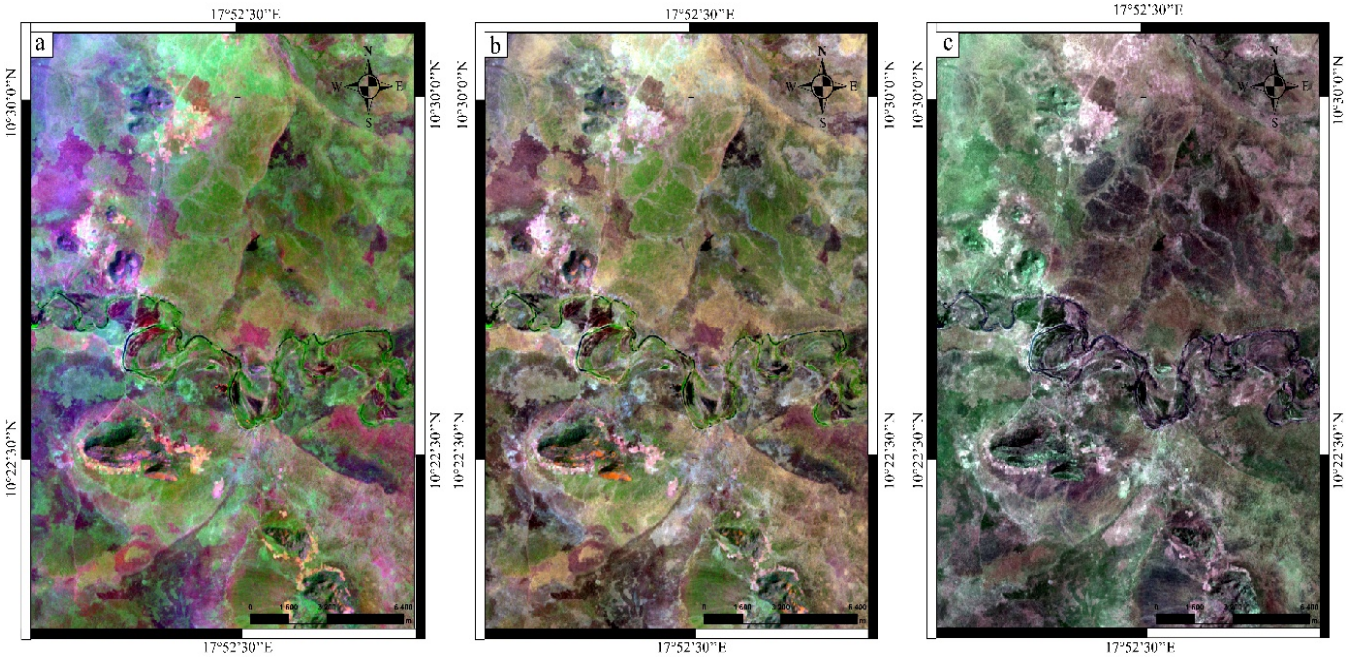

Figure 3. Color composition 751, 654and 432 of the study area

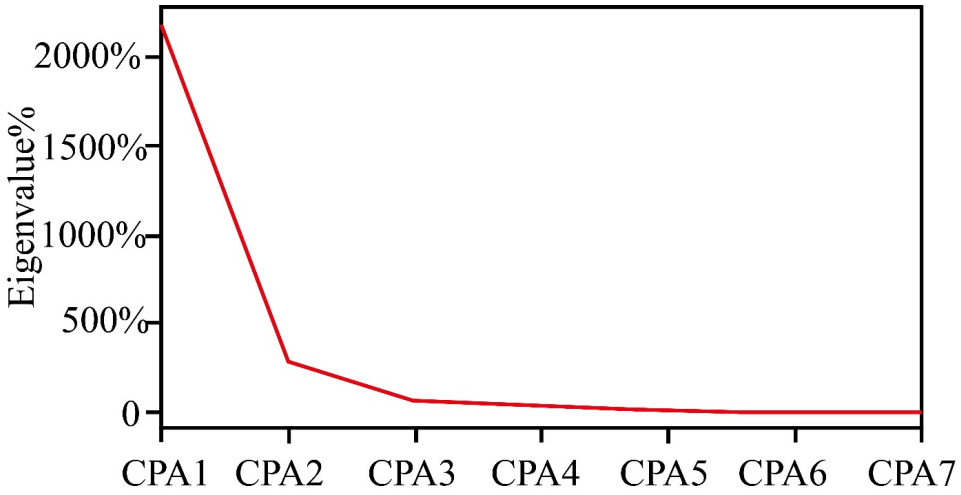

Figure 4. Percentage of eigenvalues of different bands obtained by principal component analysis (PCA)

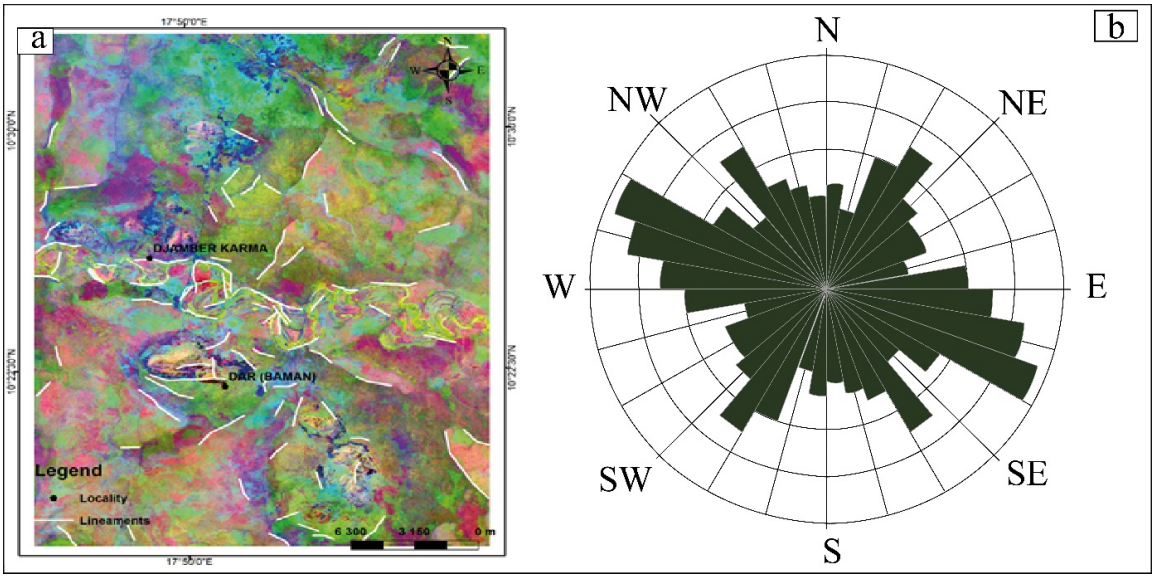

Figure 5. Lineament mapping of the North Korbol area: a lineament density map; b rose diagram of lineaments

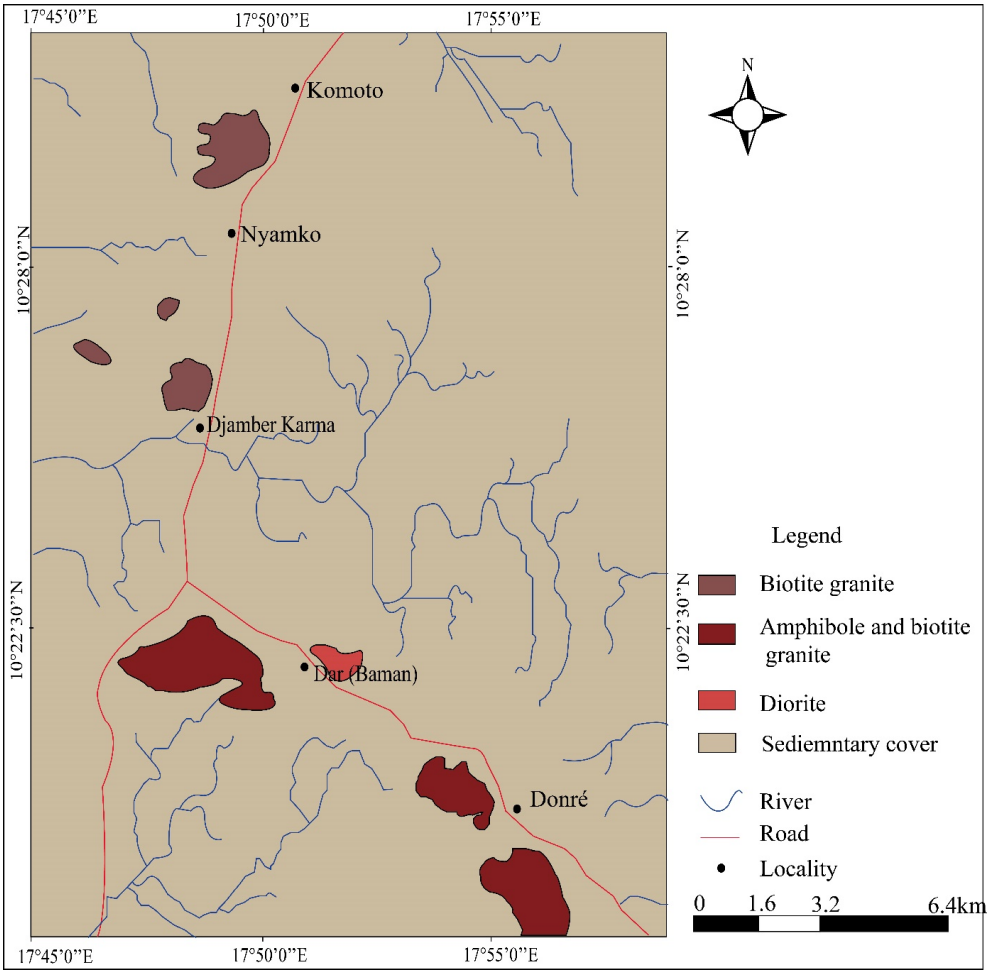

Figure 6. Geological map of the study area

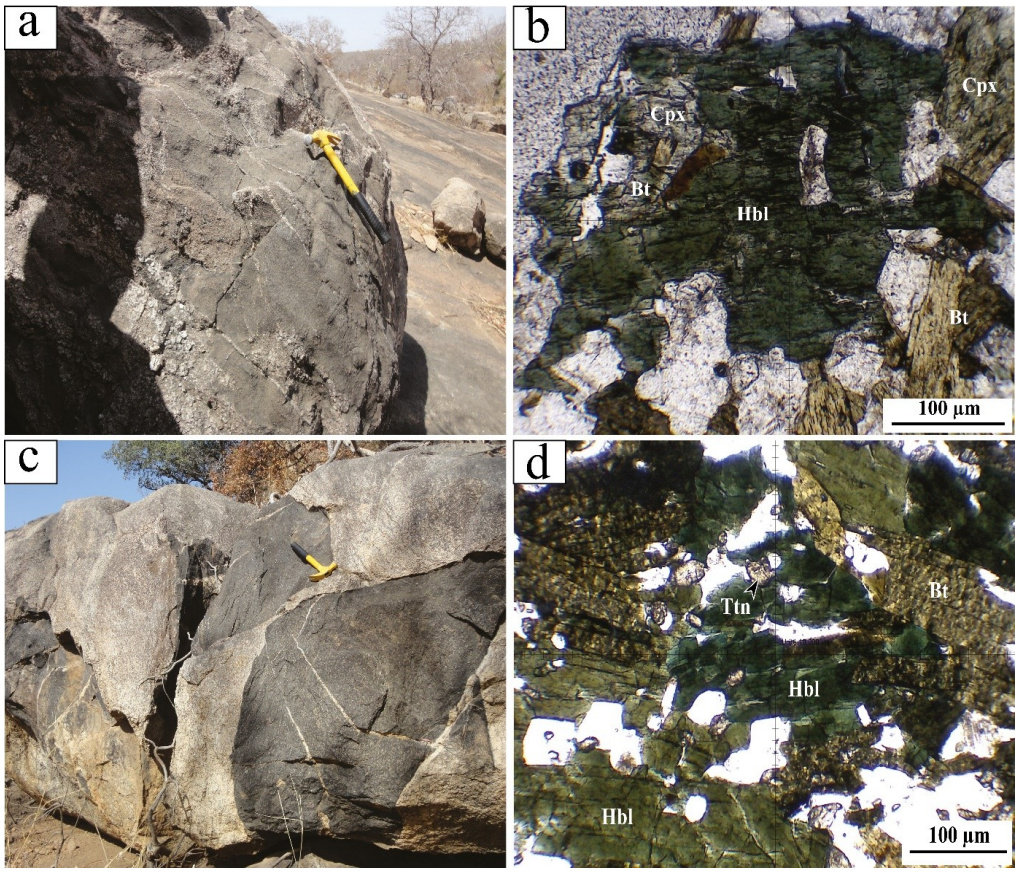

Continue …

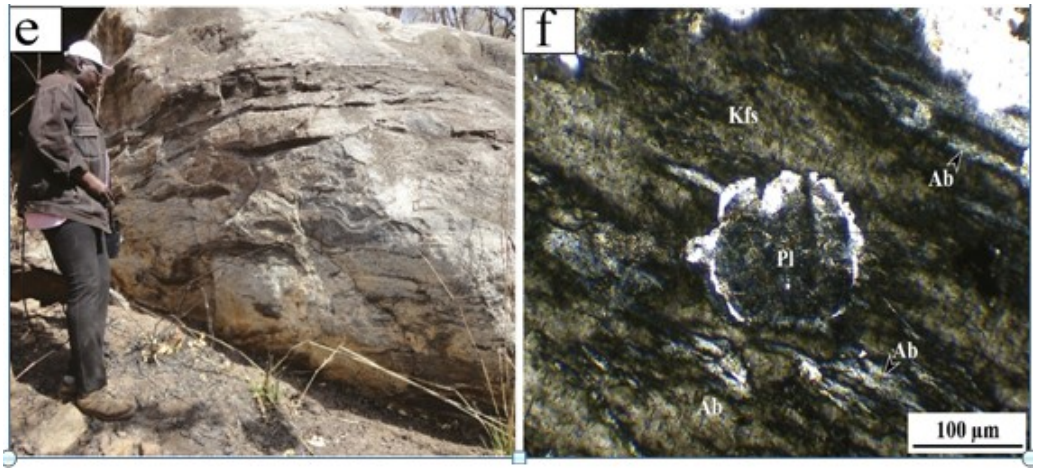

Figure 7. Photograph and microphotographs of metamorphic rocks from the study area. a) Photograph of mega enclaves of pyroxene amphibolites in biotite granites; b) microphotograph of pyroxene amphibolite showing a grouping of biotite, Cpx, and Hbl; c) photograph showing the outcrop of biotite amphibolite enclaves in granites; d) microphotograph of amphibolite showing biotite and Hbl minerals; e) photograph of the gneiss outcrop; f) microphotograph of gneiss showing Kfs, Pl, and albite minerals.

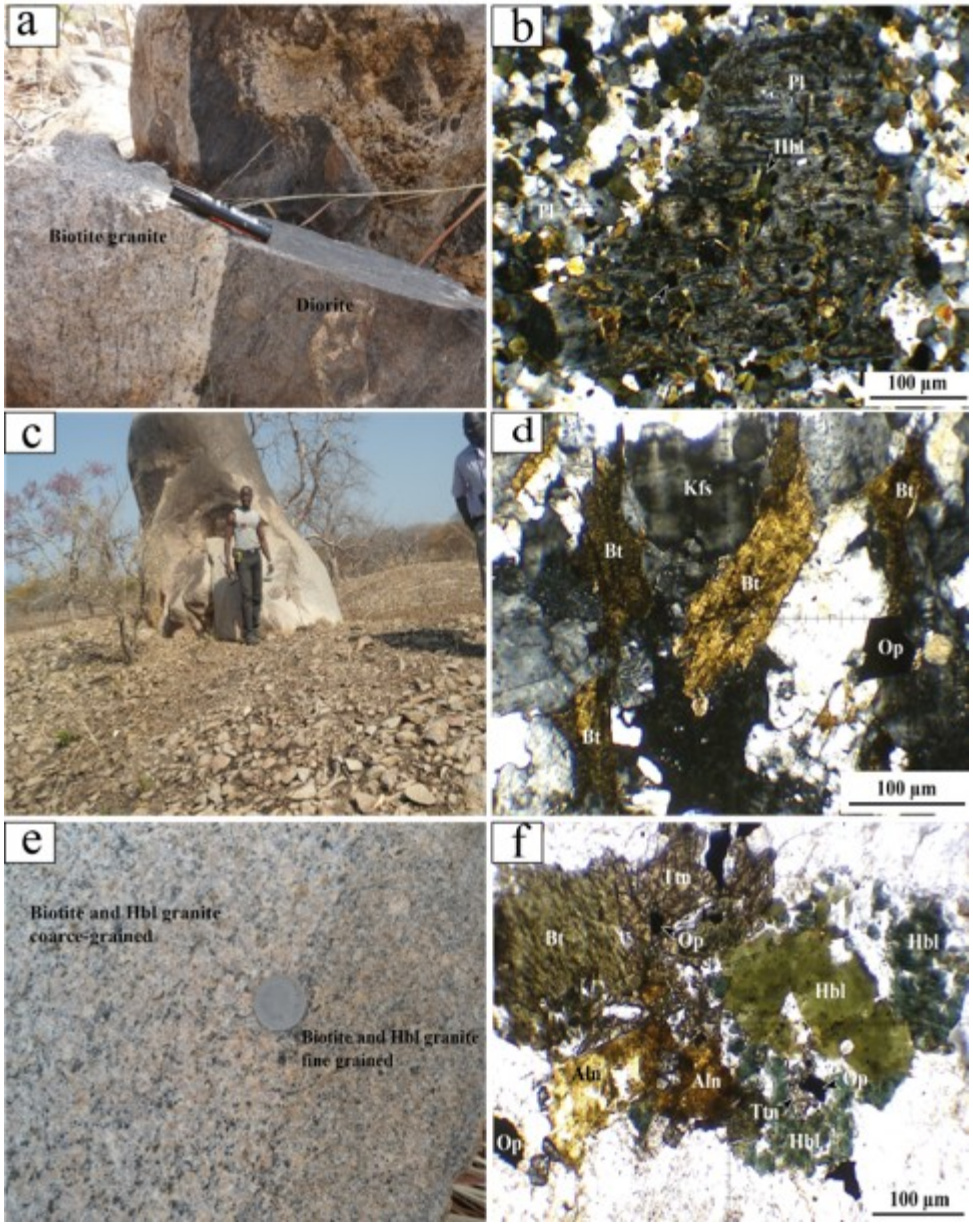

Figure 8. Photograph and microphotographs of magmatic rocks from the study area. a) Photograph of diorite showing the contact between biotite granite and diorite; b) microphotograph of diorite showing its constituent minerals; c) photograph of the biotite granite outcrop; d) microphotograph of biotite granite showing biotite flakes; e) photograph of the biotite and amphibole granite outcrop showing the contact between biotite granite and fine-grained amphibole and biotite granite and coarse-grained amphibole; f) microphotograph of biotite and amphibole granite showing biotites and amphiboles

Biotite amphibolites: Biotite amphibolite outcrops as an enclave in granites and diorites (Fig. 8a and b). The rock has a grano-nematoblastic, oriented texture and consists mainly of amphibole, plagioclase and biotite blasts in a preferential alignment. Other mineral phases include quartz, potassium feldspar, titanite, apatite, zircon and opaque minerals.

Biotite gneiss: Biotite gneiss mainly outcrops as enclaves in granites (Fig. 7e). It exhibits a grano-lepidoblastic texture highlighted by blasts of quartz, plagioclase, and potassium feldspars in the light bands. However, the dark levels exhibit biotite flakes associated with a few feldspar blasts. Accessory minerals are represented by opaque minerals, apatite, and zircon (Fig. 7f).

Diorite: Diorites outcrop in slabs or blocks, and the contact between biotite granite and diorite is diffuse. Diorites occur as mega-enclaves in biotite granites (Fig. 8a). The diorite has a porphyroid grain texture characterized by a finely grained matrix consisting of amphibole, plagioclase, potassium feldspar, apatite, zircon, opaque minerals, and biotite flakes, in which isolated clusters of plagioclase, quartz, and zoned plagioclase phenocrystals are embedded (Fig. 8b).

Biotite granite: Biotite granite mainly outcrops in massifs, slabs, or blocks (Fig. 8c) and contains gneiss and amphibolite enclaves. It has a porphyroid grain texture with a mineralogical composition consisting of potassium feldspar, quartz, plagioclase, and biotite. Accessory mineral phases are represented by apatite, zircon, titanite, and opaque minerals (Fig. 8d).

Biotite and amphibole granite: Biotite and amphibole granite outcrops in slabs or blocks (Fig. 8 e), with a diffuse contact with biotite granite and other lithological types. Biotite and amphibole granite with grains is found in clear contact with coarse-grained biotite and amphibole granite. It has a granular texture with fine-grained and coarse-grained variants. The mineralogical composition includes potassium feldspar, quartz, plagioclase, biotite, amphibole, opaque minerals, titanite, apatite, zircon, and allanite (Fig. 8f).

CONCLUSION

The use of Landsat-8 OLI combined with field data has enabled us to produce the lineament map and to distinguish the different lithological types of northern Korbol. The color composition was generated using the VNIR-SWIR bands of the Landsat 8 OLI data. As a result, the combination of bands 751, 654 and 423 of Landsat-8 OLI data was assigned as RGB images to distinguish rock formations. Principal component analysis (PCA1, PCA2 and PCA3), also in RGB mode, shows the maximum amount of information in a single image. The automatic extraction method was used to extract the lineaments. The main lineaments are characterized by ESE-WNW to NW-SE directions and a secondary NE-SW direction. Two groups of formations can be distinguished: metamorphic formations (pyroxene amphibolite; biotite amphibolite and biotite gneiss) and granitoids represented by diorites, biotite granite and biotite-amphibole granite.

Declaration of competing interests: The authors declare that they have no known competing financial interests or personal relationships that might have appeared to influence the work presented in this article.

REFERENCES

Abdelsalam, M.G., Liégeois, J.P., Stern, R.J., 2002. The Sahara metacraton. J Afr Earth Sci 34:119–136

Baïssemia, R.G., Gountié D.M., Tcheumenak K.J., Klamadji, N.M., Mbaguedjé, D., Kwékam, M., 2025. Petrography and geochemical characterization of the Baïbokoum syenitic pluton (Southern Chad): implication for the magma genesis. Acta Geochimica 44(2), 420-439. https://doi.org/10.1007/s11631-024-00733-y

Black, R., 1992. Mission géologique au Tchad du 14/1 au 08/02/1992. Rapport inédit. PNUD/DRGM, N'Djamena, 15p.

Chen, J., Zhao, Z, Yang, Y., Li, C., Yin, Y., Zhao, X., Zhao, N., Tian, J., Li, H., 2024. Metallogenic prediction based on fractal theory and machine learning in Duobaoshan Area, Heilongjiang Province. Ore Geology Rev 168:106030. https://doi.org/10.1016/j.orege orev.2024.106030

Clark, R.N., Swayze, G.A., Gallagher, A., King, T.V.V., Calvin, W.M., 1993. The U.S. geological survey, digital spectral library: version 1: 0.2 to 3.0 μm: U.S. geological survey open file report 93–592, pp 1340. http://speclab.cr.usgs.gov. August 1999

Couzinié, S., Ménot, René.-Pierre., Doumnang, J.-C., Paquette, J.-L.,Rochette, P., Quesnel, Y., Deschamps, P., Ménot, G., 2020. Crystalline inliers near Lake Iro (SE Chad): Post-collisional Ediacaran A2-type granitic magmatism at the southern margin of the Saharan Metacraton. *Journal of African Earth Sciences*, doi: https://doi.org/10.1016/j.jafrearsci.2020.103960 .

De Wit, M.J., Bowring, S., Buchwaldt, R., Fudas, F.Ö., MacPhee, D., Tagne-Kamga, G., Dunn, N., Salet, A.M., Nambatingar, D., 2021. Geochemical reconnaissance of the Guéra and Ouaddaï Massifs in Chad: evolution of Proterozoic crust in the Central Sahara Shield. South Afri J Geol, 124.2, 353-382.

Diontar, M, Doumnang, J-C., Kwékam, M., Al-hadj, H.Z., Kagou, D.A., Efon, A.J., Tcheumenak, K.J., 2020. Petrogenesis of Magnesian High-K Granitoids From Bitkine (Centre Chad Massif): Major and Trace Elements Constraints. *European* J Envi Earth Sci. 1-5. doi: http://dx.doi.org/10.24018/ejgeo.2020.1.5.89.

Diontar, M., Kwékam, M, Fozing, E.M., Kagou, D.A., Tcheumenak K.J., 2020. Petrology and Geochemical Characteristic of Granitoids From Guéra Massif in the Central Part of Chad: An Example of Mixing Magmas. Earth Sci Res, 9-2. https://doi.org/10.5539/esr.v9n2p66.

Djerossem, N.F., Berger, J, Vanderhaeghe, O., Isseini, M., Ganne, J., Zeh, A., 2020. Neoproterozoic magmatic evolution of the southern Ouaddaï Massif (Chad), BSGF - Earth Sci Bull 191, 34. https://doi.org/10.1051/bsgf/2020032.

Djerossem, N.F., 2018. Croissance et remobilisation crustales au Pan-Africain dans le Sud du massif du Ouaddaï (Tchad oriental). Thèse de Doctorat en Géosciences Environnement Toulouse. Université Toulouse-3 Paul Sabatier. 302P.

Djerossem, N.F., Zeh A., Isseini, M., Vanderhaeghe, O., Berger, J., & Ganne, J. 2021. U-Pb-Hf isotopic systematics of zircons from granites and metasediments of southern Ouaddaï (Chad), implications for crustal evolution and provenance in the Central Africa Orogenic Belt. *Precambrian Research*, 361, 1-15. https://doi.org/10.1016/j.precamres.2021.106233.

Doumnang, J-C., 2006. La géologie des formations Néoprotérozoïques du Mayo-Kebbi (S-W du Tchad). Thèse de Doctorat, université d'Orléans, 206 p

EL Makhrouf, A.A., 1988. Tectonic interpretation of Jebel Eghei area and its regional application to Tibesti orogenic belt, south-central Libya. J Afri Earth Sci 7, 945 - 967.

Genik, G.J., 1993. Petroleum geology of cretaceous-Tertiary rift basins in Niger, Chad, and Central African Republic. AAPG Bull. 77, 1389–1404. https://doi.org/10.1306/BDFF8EAC-1718-11D7-8645000102C1865D.

Guiraud, R., Bosworth, W., Thierry, J., Delplanque, A., 2005. Phanerozoic geological evolution of northern and central Africa: an overview. Journal of African Earth Sciences, Phanerozoic Evolution of Africa 43, 83–143. https://doi.org/10.1016/j.jafrearsci.2005.07.017.

Isseini, M., 2011. Croissance et différenciation crustales au Néoprotérozoïque : exemple du domaine panafricain du Mayo-Kebbi au Sud-Ouest du Tchad. Thèse de Doctorat Université Henri Poincaré, Nancy, France, 339 p

Isseini, M., André-Mayer, A.S., Vanderhaeghe, O., Barbey, P., Deloule, E., 2012. A type granites from the Pan-African orogenic belt in south-western Chad constrained using geochemistry, Sr-Nd isotopes and U-Pb geochronology. *Lithos*, 153, 39–52

Kogbe, C.A,. 1981. Cretaceous and Tertiary of the Iullemmeden Basin in Nigeria (West Africa): Cretaceous Research, 2, 129–186.

Kusnir, I., 1995. Géologie, ressources minérales et ressources en eau du Tchad, N'djaména, Centre National d'Appui à la Recherche

Kusnir, I, Moutaye, H.A., 1997. Ressources minérales du Tchad: une revue. *Journal of African Earth Sciences*, 24, 549-562.

Liégeois, J.P., 1992. Mesures des isotopes du Sr en vue de détermination d'âges des roches magmatiques du Sud du Tchad (région Baïbokoum, Léré-Figuil). Rapport inédit 10p.

Mbaguedjé, D., 2015. Métallogénie de l'or et de l'uranium dans le cadre de la croissance et de la différenciation de la croûte au Néoprotérozoïque : Exemple du massif du Mayo-Kebbi (Tchad) dans la Ceinture Orogénique d'Afrique Centrale. Thèse de Doctorat en Géosciences. Université de Lorraine. Nancy. 269P

Mbaguedje, D., Ngambi V.H., Doumnang M.JC., Allarassem L., Diontar M. 2025**.** Geological and Structural Mapping of the Ouaddaï Massif using Landsat and Radar Data , *Asian Journal of Science and Technology*, 16, (01), 13381-13387.

Mbaïtoudji M.M., 1982b. Lois de répartition, hypothèses de pronostics et méthodologie de la recherche des gisements de minéraux utiles solides dans le territoire de la République du Tchad. Institut de Prospection géologique, Moscou (URSS)

Milesi, J.P., Frizon de Lamotte, D., De Kock, G., Toteu, F., 2010. Tectonic Map of Africa: Paris, Commission de la carte géologique du monde/Commission for the Geological Map of the World (CCGM/CCGM), scale 1:10,000,000.

Nkouandou, O.F., Ngounouno, I., D´ eruelle, B., Ohnenstetter, D., Montigny, R., Demaiffe, D., 2008. Petrology of the mio-pliocene volcanism to the North and East of Ngaoundere (Adamawa, Cameroon). Compt. Rendus Geosci. 340, 28–37. https://doi.org/10.1016/j.crte.2007.10.012.

Penaye, J., Kroner, A., Toteu, S.F., Van Schmus, W.R., Doumnang, J-C., 2006. Evolution of the Mayo Kebbi region as revealed by zircon dating: an early (Ca. 740Ma) Pan-African magmatic Arc in Southwestern Chad. Afr Earth Sci 44 (4/5):530–542. https://doi.org/10.1016/j.jafrearsci.2005.11.018

Pin, C., Poidevin, J.L., 1987. U-Pb zircon evidence for Pan-African granulite facies metamorphism in Central African Republic. A new interpretation of the high-grade series of the northern border of the Congo craton. *Precambrian Research,* 36, 303-312**.**

Pouclet A, Vidal M, Doumnang JC, Vicat JP, Tchameni R (2006) Neoproterozoic crustal evolution in Southern Chad: Pan-African ocean basin closing, arc accretion and late- to post-orogenic granitic intrusion. J Afri Earth Sci, 44, 543-560.

Sadek, M.F., Ali-Bik, M.W., Hassan, S.M., 2015. Late Neoproterozoic basement rocks of Kadabora-Suwayqat area, Central Eastern Desert, Egypt: Geochemical and remote sensing characterization. Arab. J. Geosci. 8 (12), 10459–10479.

Sadek, M.F., El-kalioubi, B.A., Ali-Bik, M.W., El Hefnawi, M.A., Elnazer, A.A., 2020. Utilizing Landsat-8 and ASTER data in geologic mapping of hyper-arid mountainous region: case of Gabal Batoga area, South Eastern Desert of Egypt. Environ. Geol. 2020, 79–101.

Safianou, O., Fozing, E.M., Kwékam, M., Yaya, F., Leprince, D.A.J., 2023. Application of remote sensing techniques in lithological and mineral exploration: discrimination of granitoids bearing iron and corundum deposits in southeastern Banyo, Adamawa region Cameroon. Earth Sci Inform 1–27. https://doi.org/10.1007/s12145-023-00937-5

Safianou, O., Fozing, E.M., Tcheumenak, Kouémo J, Achu Megnemo L, Kamgang Tchuifong AB, Aman S, Mohamed R, Kwékam, M., 2024. Mapping and discrimination the mineralization potential in the granitoids from Banyo area (Adamawa, Cameroon), using Landsat 9 OLI, ASTER images and field observations. Geosyst Geoenviron 3:100239

Seguem, N., Diondoh, M., Kepnamou, A.D., Mama, N, Sami M, Alexandre, G.A., Emmanuel, E.G., 2022. Petrography and Geochemistry of Baïbokoum-Touboro-Ngaoundaye Granitoids on the Chad-Cameroon-RCA Borders (Adamawa-Yade Domain). Open J of Geol 12:136-155. https://doi.org/10.4236/ojg.2022.122007

Seguem, N. Alexandre, G.A., Klötzli, U., Kepnamou, A.D., Emmanuel, E.G., 2014. Petrography and Geochemistry of Precambrian Basement Straddling the Cameroon-Chad Border : The Touboro Baïbokoum Area. Int J Geosci 5:418-431. http://dx.doi.org/10.4236/ijg.2014.5404

Shellnutt, J., Pham, N.H.T., Yeh M.W., Lee, T.Y., 2020. Two series of Ediacaran collision-related granites in the Guéra Massif, South-Central Chad: tectonomagmatic constraints on the terminal collision of the eastern Central African Orogenic Belt. Precamb Res, doi: https://doi.org/10.1016/j.precamres.2020.105823.

Shellnutt, J., Pham, N.H.T., Steven, W., Denyszyn, M.W., Lee, T.Y., 2017. Timing of collisional and post-collisional Pan-African Orogeny silicic magmatism in south-central Chad. *Precambrian Research*, 301, 113-123.

Shellnutt, J., Pham, N.H.T., Yeh, MW., Lee, T.Y., 2020. Two series of Ediacaran collision-related granites in the Guéra Massif, South-Central Chad: tectonomagmatic constraints on the terminal collision of the eastern Central African Orogenic Belt. *Precambrian Research,* doi: https://doi.org/10.1016/j.precamres.2020.105823.

Suayah I.B., Miller J.S., Miller B.V., Bayer T.M., Rogers J.J.W., 2006. Tectonic significance of Late Neoproterozoic granites from the Tibesti massif in southern Libya inferred from Sr and Nd isotopes and U-Pb zircon data. J Afri Earth Sci 44, 561–570

Toteu, S.F., Penaye, J., Poudjom Djomani, Y., 2004. Geodynamic Evolution of the Pan-African Belt in Central Africa with Special Reference to Cameroon. *Canadian Journal of Earth Sciences*, 41, 73-85.

Wacrenier P., 1958. Carte géologique provisoire du Borkou-Ennedi-Tibesti. Brazaville, Direction de Mine et Géologie. Afrique Equatoriale Française.

Yang'tshi, M., Olola, N., Lokilo, E.L., Ngungu, M., Yang'tshi, M.N., Nzambe, K.K., Ngungu, M.B., Matamba, R.J., Kunambu, C.M., Luemba, M.L., Kalonji, G.L., Ndaye Mudumbi, H., Ngbolua, K.-T.-N., 2018. Contribution de l'Imagerie Landsat 8 dans le repérage et la cartographie des linéaments aux environs de Madimba, dans l'Ouest Congolien (Kongo Central, République Démocratique du Congo). Int. J. Innov. Sci. Res. 38, 192–202.

Zhao Z, Zhao X, Yin Y, Li C, Yang Y, Wang Y., 2024. Identification of geochemical anomalies based on RPCA and multifractal theory: a case study of the Sidaowanzi Area, Chifeng, Inner Mongolia. ACS Omega 9:24998–25013. https://doi.org/10.1021/acsomega. 4c02078

****